ELSEVIER

Physics of the Earth and Planetary Interiors 92 (1995) 169–187

PHYSICS OF THE EARTH AND PLANETARY INTERIORS

# Frequency–moment distribution of deep earthquakes; implications for the seismogenic zone at the bottom of slabs

Emile A. Okal [a,*], Stephen H. Kirby [b]

[a] *Department of Geological Sciences, Northwestern University, Evanston, IL 60208, USA*
[b] *US Geological Survey, Menlo Park, CA 94025, USA*

Received 29 November 1994; revision accepted 4 April 1995

**Abstract**

We present a systematic investigation of the variation with depth of the frequency of earthquake occurrence vs. seismic moment based on 16 years of Harvard Centroid Moment Tensor (CMT) solutions. We analyze depth variations of earthquake size distribution in terms of variations in the absolute value of the slope of the regression of the logarithm of the population vs. seismic moment, a quantity known as the $\beta$ parameter. The shallowest earthquakes (0–50 km depth) exhibit a well-defined and robust size distribution regime characterized by a discontinuous increase in $\beta$ with increasing moment. Others have shown that this increase probably represents the effects of a physical limit in the dimensions of the area of seismogenic slip of shallow earthquake sources. The population of deep earthquakes in the depth interval 500–600 km shows two markedly different distributions. The deep earthquakes in the Tonga region feature an initially high $\beta$ value (0.92) at small moments and a lower $\beta$ value (0.41) at high moments. In contrast, the size distribution of non-Tonga deep events shows the reverse of those changes ($\beta = 0.41$ at low moment and $\beta = 1.17$ at higher moment). To help explain these observations, we propose a model of deep seismogenesis that assumes three-dimensional earthquake source regions that vary principally in their transverse dimensions. The two-$\beta$ segment behavior in the Tonga region and other subduction zones is thought to represent, in part, constraints owing to the threshold of completeness of the CMT catalog and to its short time interval of sampling. We interpret the differences between Tonga and other deep Wadati–Benioff zones as being a consequence of Tonga's markedly higher subduction rate and, hence, its colder thermal structure and presumably thicker region of seismogenesis. We interpret the critical moments at which $\beta$ values change in terms of variations in the transverse thickness of deep seismogenic zones and estimate that it is about 11 km for the Tonga region and about 3 km for other zones at depths of 500–600 km. These results are generally consistent with deep earthquakes being restricted to wedge-shaped regions of peridotite persisting metastably to as deep as 700 km in old, rapidly descending and hence cold slabs. Failure is thought to occur in metastable peridotite by transformational faulting. Great deep earthquakes present special challenges to any theory of deep earthquakes based on slab thermal structure. For example, a continuing question is how such large events can fit in a thermally controlled seismogenic zone that is diminishing in its transverse dimensions with increasing depth. The very concept of a scale-invariant earthquake size distribution may be inappropriate for these rare events and the unusual settings in which they are found.

* Corresponding author.


*SSDI* 0031-9201(95)03037-9

## 1. Introduction

A significant limitation on the sizes of earthquakes is placed by the finite physical dimension of seismogenic zones. All other factors (such as material properties) being equal, the smaller the area available for rupture, the smaller the maximum earthquake size. An excellent example of this limitation is the effect of very thin and hot lithosphere at mid-ocean ridges and at short-offset transform faults: net seismic moment release rates (Frohlich and Apperson, 1992) and maximum seismic moments (Burr and Solomon, 1978; Okal and Stein, 1987) tend to be low in these settings, even at fast-spreading ridges. The spatial dimensions of seismogenic zones may be estimated directly from the distribution of earthquake hypocenters and from the mapping of slip regions inferred from seismic source tomography (e.g. Houston, 1987). Those approaches, although useful in some settings, may be limited where exclusively teleseismic constraints are placed on hypocenter depth distribution, where earthquakes are infrequent, and where inversions for slip dimensions are non-unique or poorly constrained by independent observations, such as aftershock distributions. Such limitations on the investigation of the dimensions of the seismogenic zone are especially severe for deep earthquakes, because the latter generally do not have abundant aftershocks, and waveform inversions for fault dimensions may be biased by marked lateral seismic velocity heterogeneities in the vicinity of slabs.

Another approach is to investigate the variation of earthquake populations with magnitudes or moments: as earthquakes increase in size and faulting area, they may reach dimensions comparable with those of the seismogenic zone, and hence, earthquake numbers above that size may drop off more rapidly than predicted for a spatially unbounded region. Such a physical saturation of the faulting area within the seismogenic zone has been suggested by two recent investigations (Pacheco et al., 1992; Romanowicz and Rundle, 1993) of shallow earthquakes. Pacheco et al. (1992) also suggested that the saturation size may be smaller for intermediate and deep earthquakes. In addition, a recent phase-change theory of deep earthquakes within subducting slabs suggests that deep shocks may be restricted to the cores of the coldest slabs (Kirby et al., 1991, 1995b) and hence to a fraction of the thickness of slabs which decreases with increasing depth. Our paper probes further into this question of the dimensions of deep seismogenic zones through an extended analysis of the deep earthquake size–frequency relationships, and by comparison of its results with theoretical estimates of the dimensions of deep seismogenic zones.

## 2. Background

An interesting development in our understanding of the nature and extent of seismic faulting has come recently from a number of studies focusing on frequency–magnitude relationships, such as those by Pacheco et al. (1992) and Romanowicz and Rundle (1993). These workers have observed a change in the slope of the frequency–magnitude relation (the so-called $b$ value) for large earthquakes, which they have interpreted in terms of the physical saturation of the width of the fault. Okal and Romanowicz (1994) have shown that the problem is compounded by the variation in magnitude–moment relationship, and recommended the use of a frequency–moment analysis to single out the physical saturation of the fault dimension, independently of the intrinsic saturation of any conventional magnitude scale owing to the finiteness of the wavelengths involved (Geller, 1976). Thus, we will characterize earthquake populations by a $\beta$ value, such that the number $N$ of earthquakes in the population with moments equal to, or greater than, $M_0$ is

$$\log_{10} N = a - \beta \log_{10} M_0 \qquad (1)$$

(In all equations in this paper, $a$ will be taken as a constant, whose values are unrelated in subsequent equations.) This notation was introduced by Molnar (1979). In the case of shallow earthquakes, and as detailed by Rundle (1989), Romanowicz and Rundle (1993) and Okal and Ro-

manowicz (1994), one predicts $\beta = 2/3$ under the assumption that the source scales at constant stress drop.

This value is upheld spectacularly well at lower moments for extensive datasets of shallow earthquakes, such as the Harvard Centroid Moment Tensor (CMT) catalog. However, for large moments, a significant increase in $\beta$ value is present, and can be explained by a saturation of the fault width $W$ (which cannot keep increasing outside the boundary of seismogenic material), and of a concurrent limitation of the slip $\Delta u$ (Romanowicz and Rundle, 1993). The critical moment $M_0^c$ at which saturation is reached (approximately $2 \times 10^{27}$ dyn cm) can be used to infer the maximum fault width, and in turn, the thickness of the seismogenic zone.

In the case of deeper events, Pacheco et al. (1992) have similarly studied two populations of 'intermediate' and 'deep' earthquakes. Their work used $b$ values computed on the moment magnitude $M_w$; equivalent $\beta$ values are obtained through multiplication by two-thirds. Pacheco et al. claimed a change of behavior for both intermediate and deep earthquakes around $M_w = 6.5$, corresponding to $M_0^c = 7 \times 10^{25}$ dyn cm. However, these workers used only a traditional sorting of earthquakes in three depth bins (shallow, intermediate and deep, separated at depths of 100 and 300 km—in their text; the caption to their Fig. 3 indicates equal to or less than 70 km, 100–350 km and equal to or greater than 350 km). Considerable evidence indicates more subtle changes in the regime of seismicity with depth, and in particular a strong increase in the level of activity around 450–500 km, and thus the question arises of the robustness of their results with respect to a change in binning depths. Also, Pacheco et al. (1992) did not discuss the choice of $M_0^c$ used to position the change in slope.

In an earlier paper, Giardini (1988) studied systematically the geographical variation of $b$ values for deep earthquakes, and identified the Tonga–Kermadec area as featuring very high $b$ values. However, his depth parameterization remains coarse, and furthermore, his dataset consists fundamentally of the International Seismological Centre (ISC) catalog, with events quantified through their body-wave magnitudes $m_b$, even though Giardini expressed them as moment magnitudes $M_w$; this casts some doubt on the homogeneity of the dataset, given the poor correlation between high-frequency magnitudes and seismic moments for even moderately large earthquakes (e.g. Okal, 1992).

More recently, Frohlich and Davis (1993) included the CMT dataset among the many populations they studied, but restricted their analysis to a narrow range of magnitude $M_w$, corresponding to $24.6 \leqslant \log_{10} M_0 \leqslant 25.9$. They similarly identified the Fiji–Tonga–Kermadec area (which they called 'Tonga–Fiji') as featuring anomalously high $b$ values. Both Giardini and Frohlich and Davis used the traditional sorting of earthquakes with depth (with boundaries at 70 and 300 km). The question of the anomalous behavior of earthquakes in the Tonga slab is of great interest, in view of the recent reassessments of the rate of convergence at the Tonga subduction zone (Bevis et al., 1991, 1993), which give it the largest values of age (approximately 140 Ma; Engebretson et al., 1991) and convergence rate (up to 22 cm year$^{-1}$), two parameters governing critically the thermal regime and degree of metastability of the subducted lithosphere in the slab (Kirby et al., 1991).

In this context, the purpose of the present study is to investigate systematically the variation of $\beta$ value with depth using the CMT catalog (1977–1992), and to search for robustness and consistency in the results upon variation of the binning procedure, as well as exploring systematically the question of the anomalous behavior of the Tonga region.

We realize that the relative youth (16 years) of the CMT catalog is somewhat of a disadvantage, especially regarding large earthquakes, which are significantly under-represented in the catalog at all depths. It is, however, the only available catalog of physical descriptors of the source of deep earthquakes, based on homogeneous measurements obtained through a common algorithm for all events. In addition, most of the truly very large deep earthquakes (Peru, 1922; Spain, 1954; Colombia, 1970; and now Bolivia, 1994) have occurred as spatially isolated events, and it is not clear that they share with other populations the

scale independence expressed by a constant $\beta$ value.

## 3. β Value investigations of the CMT dataset

### 3.1. The global catalog as a function of depth

We start by simply considering arbitrary bins of 100 km width for the centroid depths, as published in the CMT catalog (Fig. 1). In this and all similar figures, we use bins with a width of 0.1 unit of $\log_{10} M_0$; the plus signs represent the number of earthquakes within each bin; the larger symbols the cumulative number of events in the bin or larger. The regressions defining the $\beta$ values are carried on the cumulative numbers and different symbols are used for different regression segments. The open circles (mostly at the lower end of the moment scale) represent events not used in the regression because of incompleteness of the dataset. The figures also show the standard deviations of the coefficients $\beta$, computed with identical weights assigned to all bins.

The resulting regressions would suggest the following picture: (1) as described in previous

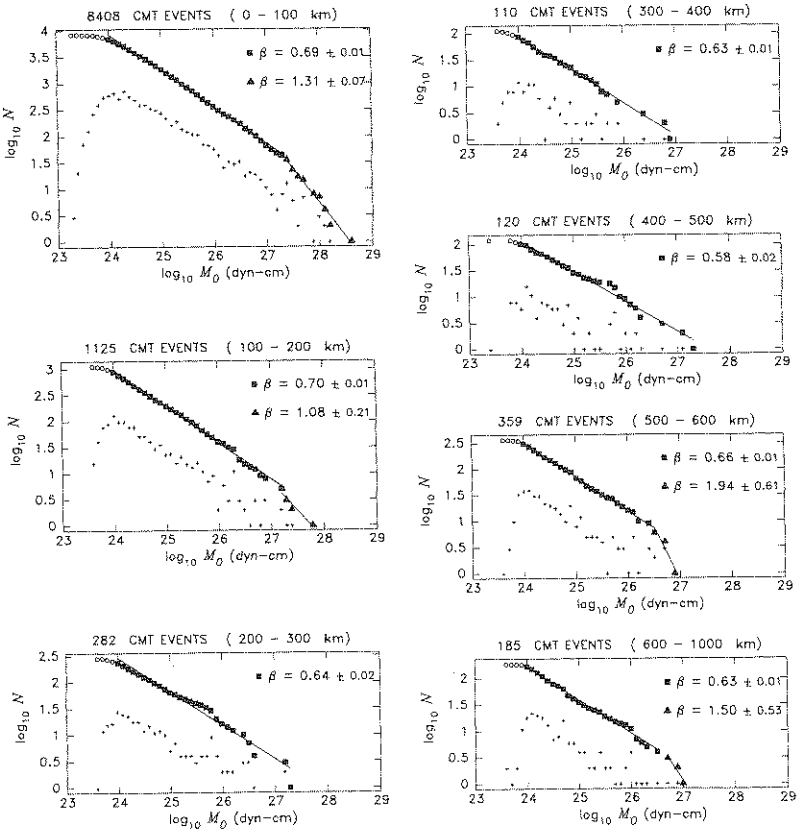


Fig. 1. $\beta$ Value regressions of the CMT dataset binned into 100 km depth intervals. In this and all similar figures, the width of the sorting bins is 0.1 unit of $\log_{10} M_0$. Individual crosses represent the number of earthquakes in each bin; other symbols relate to $N$, the cumulative number of events with moments equal to or greater than $M_0$. $\beta$ Values are obtained by fitting a straight line to $\log_{10} N$ over specific ranges of moment. Different symbols are used for different ranges, and the corresponding value of $\beta$ printed on the right. Open circles denote parts of the dataset not used in the regressions, principally at low moment ranges, where the completeness of the dataset would be questionable. In all cases, the figures are log–log plots with common scales, so that $-\beta$ is always the true slope of the regression on the figure. The total population is printed as part of the title of each frame.

studies, the 0–100 km bin follows the two-thirds slope remarkably well, with $\beta$ increasing to greater values beyond the critical moment; (2) a very similar behavior is found for very deep earthquakes in the 500–600 km range, but with a lower value of the critical moment: $\log_{10} M_0^c = 26.7$ (note that this value is larger than proposed by Pacheco et al. (1992), by about 0.9 unit); (3) at those depths where the level of seismic activity is lowest ($200 < h < 500$ km), $\beta$ value regressions suggest slopes close to two-thirds, but the quality of fit is poor, with an occasional hump in the curve around $\log_{10} M_0^c = 25.6$; (4) the 100–200 km bin has a behavior intermediate between (1) and (3); (5) the very deepest earthquakes ($h > 600$ km) seem to follow behavior (2), but with a significant deterioration of the fit, reminiscent of (3). Finally, it is important to bear in mind that several datasets have very meager populations, with only about 100 samples in two of the bins.

To assess the robustness of these results, we quantify the significance of a change of slope by considering the variance reduction $VR$ (or improvement in the goodness of fit, $\sigma$) brought

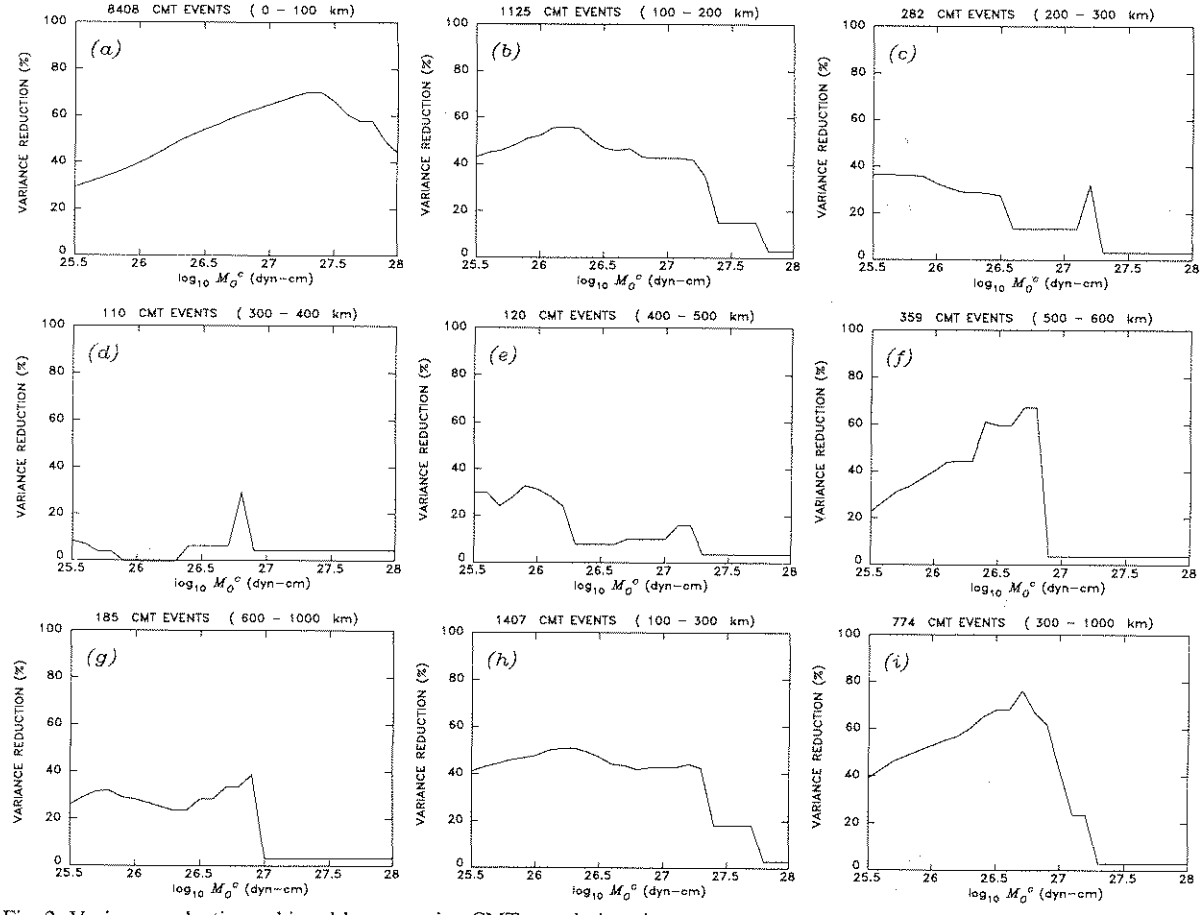


Fig. 2. Variance reduction achieved by regressing CMT populations into two segments, as opposed to one segment, plotted as a function of the position of the critical moment $M_0^c$. The quantity plotted is $VR$, as defined in Eq. (2). (a)–(g) Depth bins of 100 km used in Fig. 1. (h), (i) Depth bins used by Pacheco et al. (1992) to define their populations of intermediate and deep events. (See text for interpretation.)

about by regressing the dataset in two segments intersecting at $M_0^c$ rather than in a single segment:

$$VR = 1 - \frac{\sigma_2}{\sigma_1} \quad (2)$$

where the goodness of fit, $\sigma$, is expressed in both cases as the root-mean-squares residual of the actual population with respect to its modeled value (using one segment for $\sigma_1$, and two for $\sigma_2$).

In Fig. 2, we formally study $VR$ as a function of $M_0^c$ for the various depth bins. Only two substantial peaks in $VR$ are present: one at $\log_{10} M_0^c = 27.3$ for shallow events, and one at $\log_{10} M_0^c = 26.7$ in the 500–600 km depth bin. On the other hand, the plot for 100–200 km, for example, means that, although a fair degree of variance reduction is achieved by regressing the dataset in two segments, the quality of the fit is basically independent of the position of the elbow: that simply describes a dataset with continuous curvature; a similar conclusion would be reached when using the 100–300 km bin used by Pacheco et al. (1992) for 'intermediate' earthquakes. On the other hand, the 300–400 km plot indicates no variance reduction, as expected from Fig. 1, which showed a relatively good fit by a single straight line in the first place. Finally, when combining all 'deep' events below 300 km, the very deep seismicity controls the behavior of the dataset, giving rise to a sharp peak in $VR$ at $\log_{10} M_0^c = 26.7$, the latter providing a better fit than proposed by Pacheco et al. (1992), using $\log_{10} M_0^c = 25.8$.

We regroup these results in Fig. 3, where we plot in the left frame the best variance reduction achieved as a function of depth, and in the center frame the critical moment providing this best fit. We keep track of the population of the depth bins in the right frame. We further investigate how robust these results are with a change of model, namely by changing the width of the depth bins: we use a continuous line for 100 km bins, long dashes for 75 km bins and short dashes for 50 km bins. Not surprisingly, we find that the results for shallow earthquakes (0–50 km) are most robust: a critical moment of $2 \times 10^{27}$ dyn cm and a variance reduction of 70% are achieved in all cases. The only other region featuring apparently robust results (i.e. where the three types of curves are superimposed) is between 525 and 600 km, where in all cases, we obtain $VR \geq 60\%$, and a consistent $M_0^c = (5\text{–}6) \times 10^{26}$ dyn cm. Else-

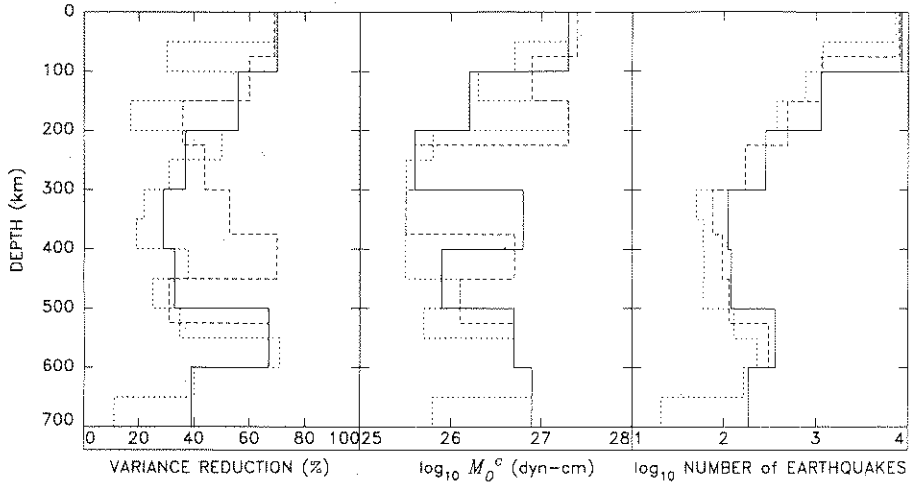


Fig. 3. Optimal variance reduction (left), corresponding critical moment (center), and bin populations (right), plotted as a function of depth for various binning strategies (continuous line: 100 km bins; long dashes: 75 km bins; short dashes: 50 km bins). Robustness is indicated by the coincidence of the various types of lines. (Note that only the results for 0–50 km and 525–650 km are reasonably robust.)

where, the optimal moment, as well as the level of variance reduction, are not robust, and depend on the particular binning used. This is easy to understand in the 250–500 km range, where the populations studied are very small. The unstable behavior between 100 and 250 km is on the other hand surprising and at present we do not have a simple explanation for it.

### 3.2. The particular case of the deep Tonga earthquakes

Motivated by the studies of Giardini (1988) and Frohlich and Davis (1993), we next address the question of the Kermadec–Tonga–Fiji dataset. We define as 'Tonga' those events taking place in the region delimited by latitudes 14°S and 42°S, and longitudes 175°E and 170°W. There are 1560 Tonga events in the 1977–1992 CMT catalog (15% of the global dataset), of which 377 have a depth of 500 km or more (69% of the deep global dataset). In this section, we carry out $\beta$ value regressions both for 'Tonga' and 'non-Tonga' datasets, in the depth bins (0–50 km and equal to or greater than 500 km) identified above as providing robust results on the global dataset.

In the shallow domain (0–50 km), we find that the behavior of the non-Tonga events is similar to that of the global dataset (which is not surprising, as they dominate the population (6444 events, or 89% of the total), whereas the Tonga group has a rather erratic frequency–size relationship: the best two-segment regression requires $\log_{10} M_0^c = 27.3$, but provides only 26% variance reduction. The shape of the curve suggests that the dataset may not be homogeneous, but rather may result from the superposition of two independent populations.

The most interesting situation occurs for the deep dataset ($500 < h < 600$ km). Fig. 4(a) shows that a global regression indicates a behavior totally similar to that of shallow earthquakes: $\beta = 2/3$ below a critical moment of about $5 \times 10^{26}$ dyn cm, followed by a sharp increase in $\beta$. However, Figs. 4(b) and 4(c) reveal that this behavior is a total artifact of the superposition of two very different datasets: the 'Tonga' earthquakes exhibiting a higher $\beta$ value (0.92) followed by a decrease ($\beta = 0.41$) beyond $\log_{10} M_0^c = 25.8$, and the remainder of the deep population, or 'non-Tonga' events, showing $\beta$ values initially very low (0.41), and increasing to about unity beyond $\log_{10} M_0^c = 25.9$. As such, it would certainly be erroneous to take the tempting step of providing a physical interpretation of the parameters suggested by Fig. 4(a) (for example, by relating the apparent critical moment to a physical dimension of the seismogenic zone), while the other two frames prove convincingly that such a model would apply nowhere—neither in the Tonga area, nor outside it!

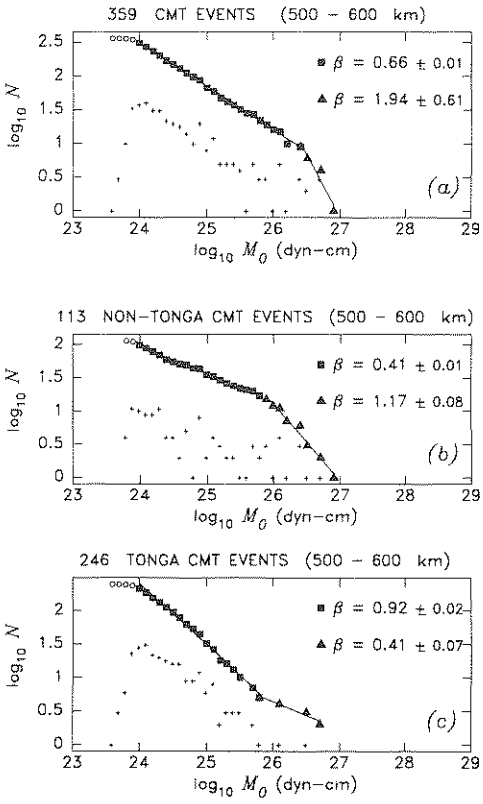


Fig. 4. $\beta$ Value regression results for (a) the global dataset of 500–600 km earthquakes; (b) only those events from subduction zones other than Tonga, and (c) only those events from the Tonga area as defined in the text.

At greater depths ($h \geq 600$ km), the Tonga population has an uneven frequency–moment distribution exhibiting significant misfit by a single straight line. In view of this situation, we split

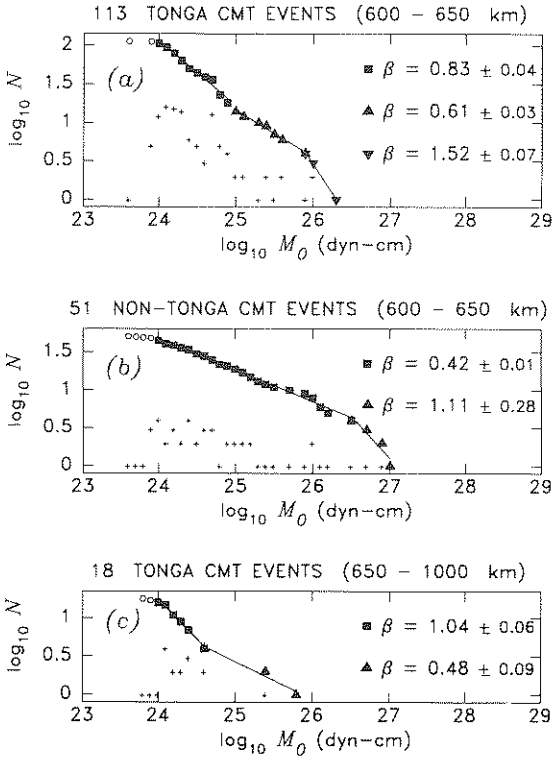


Fig. 5. (a) $\beta$ Value regression of the Tonga population of events in the 600–650 km range; (b) regression for events from other subduction zones; (c) tentative regression for Tonga events below 650 km.

it further by considering the two depth bins 600–650 km and 650 km or greater. The 600–650 km population can be modeled in three segments (Fig. 5(a)) with slopes approaching unity, one-half, and more than unity with critical moments of $8 \times 10^{24}$ and $8 \times 10^{25}$ dyn cm, and there is some indication of a change of regime from $\beta = 1$ to $\beta = 0.5$ around $4 \times 10^{24}$ dyn cm for the very deepest earthquakes ($h \geq 650$ km; Fig. 5(c)). However, given the population involved (18 events in the latter case), this constitutes no more than a speculative argument.

As for the non-Tonga population below 600 km, it can be regressed in two segments, articulated at $3 \times 10^{26}$ dyn cm, and with slopes approaching one-half and unity (Fig. 5(b)). As there are only three events below 650 km, it is not possible to split the dataset further.

An attempt to regionalize further the latter dataset did result in the identification of several potentially interesting trends, but involved such low populations (typically 20–30 events) as to render their significance doubtful.

### 3.3. Summary of results

We can summarize our results as follows:

(1) the two-segment behavior ($\beta = 2/3$ followed by $\beta \geq 1$) described by Pacheco et al. (1992) and Romanowicz and Rundle (1993) for shallow earthquakes is not robust below 50 km depth.

(2) A similar two-segment regression cannot be achieved robustly in any other depth bin. In particular, for the intermediate region (100–300 km) as proposed by Pacheco et al. (1992), it does not resolve the value of the critical moment. The only potential candidate would have been the 500–600 km depth band, but we have shown that two subpopulations (Tonga and non-Tonga) have widely differing behaviors.

(3) The deep Tonga earthquakes ($500 < h < 600$ km) exhibit a strikingly different behavior ($\beta \approx 1$ followed by $\beta \approx 1/2$). It should be noted that the latter behavior remains tentative, as it is entirely defined by an extremely small group of only five events. As depth is increased beyond 600 km, there is some evidence of a decrease in the critical moment separating those two regimes, and of the development of a third regime ($\beta \geq 1$) at the high-moment end.

(4) The deep non-Tonga earthquakes show yet another behavior, with $\beta$ close to one-half even for the smallest events, and a suggested increase to $\beta = 1$ around $10^{26}$ dyn cm. There is no detectable change of behavior at 600 km, but the dataset for $h \geq 600$ km becomes very small (54 events).

## 4. Interpretation

We believe that, rather than expressing fundamentally different processes, the difference in behavior between Tonga and non-Tonga events is primarily a question of scaling of the seismogenic

zone, and of the absolute level of seismicity, in the context of two limitations inherent in our $\beta$ values investigations: our inability to count fewer than one earthquake in a bin, and the threshold of completeness of the CMT catalog (at present $10^{24}$ dyn cm).

We propose in this section a population model for all deep earthquakes exhibiting a three-tier behavior, namely $\beta = 1$ at small moments, followed by $\beta = 1/2$ for events of an intermediate size, followed by a return to $\beta = 1$ for the larger earthquakes (see Fig. 7(a), below). As detailed further below (and similarly to the case of shallow earthquakes), the transition moments are controlled by the dimension of the seismogenic zone, which in turn reflect the thermal structure inside the slab, itself controlled by the age and velocity of the subducting lithosphere. Hence the striking difference between Tonga (by far the fastest-sinking slab), and all other slabs.

We recognize that the proposed model is a combination of several hypotheses of a tentative (some would say speculative) character. However, we believe that it provides an interesting framework explaining some of the major features of earthquake size distributions just described.

### 4.1. Adapting Rundle's model to deep earthquakes

We start with Rundle's (1989) population model in the case of shallow events. Its success lies in the relative simplicity of the two fundamental assumptions it uses to derive the Gutenberg–Richter frequency–magnitude relation: (1) the number of earthquakes of a given size is inversely proportional to their area of faulting: $N = a/S$; (2) in the absence of saturation of the size of the faulting area, earthquakes scale at constant aspect ratio of the fault zone ($L/W =$ constant) and constant stress drop (i.e. $\mu \Delta u/W$ = constant). This results in $M_0 = aS^{3/2}$, and therefore in $\beta = 2/3$.

In Rundle's (1989) words, the first assumption amounts to saying that 'the fault area available to produce events of all sizes is the same', which can also be taken as expressing that the process of rupture along the seismogenic fault zone is scale independent. In more general terms, this assumption requires that $N$ be inversely proportional to the spatial extent of the seismogenic zone over which stress is released, and which is therefore no longer available for seismic rupture in the next event of comparable size. Of course, in the case of shallow events, occurring on well-defined fault zones, the seismogenic zone is two-dimensional, and its characteristic dimension will be the area of rupture $S$. The scale independence of rupture results in the population having a fractal dimension (Turcotte, 1992), which is easily shown to be $F = 2$.

In the case of deep earthquakes, we keep the basic philosophy of Rundle's successful model, but we propose that the seismogenic zone is three-dimensional, so that its characteristic size will be its volume $V$, and its fractal dimension, $F = 3$. It is, arguably, difficult to compare the spatial distribution of deep vs. shallow earthquakes, if for no other reason that for the latter, the proximity of the surface makes it possible to operate dense seismic networks in their immediate proximity, and to refine our three-dimensional estimates of their location to a precision occasionally reaching a hundred meters or less. Conflicting data exist regarding the spatial characteristics of the aftershocks of deep earthquakes, a situation aggravated by their rarity: an extensive compilation by Willemann and Frohlich (1987) suggests that they tend to occur in random directions from the main shock, whereas a detailed study of the recent deep Fiji event by Wiens et al. (1994) shows a clustering along the fault plane.

On the basis of a dataset of ISC solutions, in a limited magnitude range, and based on $m_b$ magnitudes, Giardini (1988) has proposed that the fractal dimension of the Tonga seismic zone may be $F = 2.4$. We prefer the integer number three, which is easier to interpret, and as we will see, predicts an exact $\beta = 1$.

The fact that, despite their higher fractal dimension, most deep earthquakes are nevertheless satisfactorily modeled by a double-couple (or by a combination of double-couples for events with so-called non-double-couple components) suggests that the concept of a faulting area and the relation $M_0 = \mu S \ \Delta u = \mu LW \ \Delta u$ both remain

appropriate at depth. On the other hand, $V$ will represent the extent of the zone surrounding the shock over which stress release is sufficient to inhibit seismogenesis of the next event; it will be expressed as $V = LWD$, with $D$ representing a dimension transverse to the fault plane.

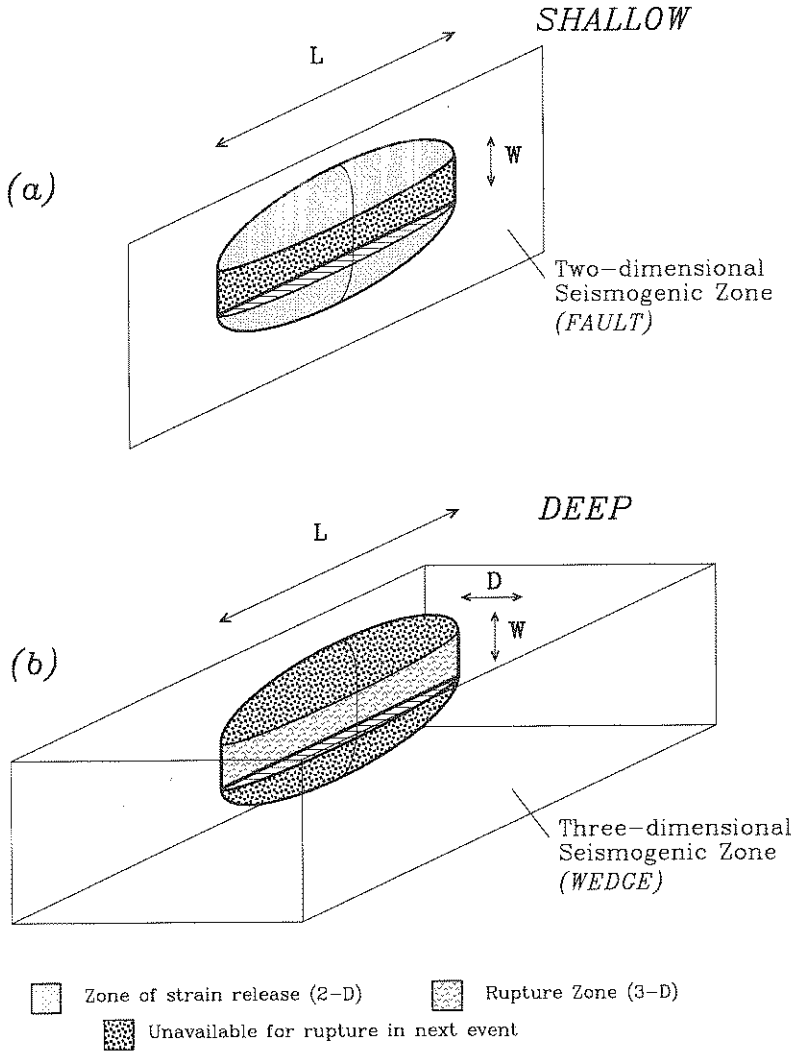


Fig. 6. Sketch illustrating the proposed differences in the fractal geometry of the source regions for shallow (a) and deep (b) earthquakes (assuming small events for which no physical saturation takes place). In the shallow case, the seismogenic zone is a two-dimensional fault (sketched as the light rectangle); in the deep case, it becomes a three-dimensional wedge (sketched as the light parallelepiped). In both cases, the submarine-shaped zone represents the three-dimensional region over which the coseismic stress release takes place (or reaches a high enough threshold). In both instances, the zone unavailable for earthquake rupture in the next event is shown densely dotted. It is obtained by taking the mathematical intersection of the region of (sufficient) stress release with the seismogenic zone: for shallow events, it is simply the rupture zone itself (a); for deep events, it is the whole zone of stress release (b). In both instances, the surface of the submarine has been carved out along a narrow band to expose the rupture zone.

We propose to keep the concept of scaling of the seismic source. This concept is based on the existence of invariants, such as the general shape of the area of rupture, and the maximum strain allowed in the medium before rupture. For a three-dimensional seismogenic zone, the parameters $D$ and $W$ will both scale as $L$, the main dimension of the rupturing area, so that in the end, the dimension $V$ of the region affected by the rupture will scale as $L^3$, rather than $L^2$ for shallow events on a fault. Let us emphasize that the difference between the two models is not in the nature of the zone of stress release, but rather in that earthquake sources are allowed anywhere (in three dimensions) in the seismogenic zone for deep events, but only on a two-dimensional fault for shallow shocks. Our proposed model is sketched in Fig. 6.

If $N$ scales as $L^{-3}$ for deep events, then, as $M_0 = aL^3$, one infers $N = aM_0^{-1}$ and therefore $\beta = 1$. This is in agreement with our observation in Tonga for smaller events between 500 and 600 km ($\beta = 0.92$), and this situation is expected to occur as long as the dimension of the zone of stress release does not exceed the size of the seismogenic zone. In the model of Kirby et al. (1991), the seismogenic zone would be the cold tongue of metastable peridotite in which transformational faulting can take place.

Finally, it is interesting to note that, apart from the case of deep earthquakes, values of $b$ significantly higher than the world-wide average ($b = 0.9$) are documented during certain episodes of volcanic seismicity (e.g., Minakami, 1974), this property having been used to interpret volcanoseismic swarms in the absence of direct observation, notably for underwater sources (Talandier and Okal, 1987). The situation may be obscured by the fact that the magnitudes in question (usually $m_b$ or $M_L$) may intrinsically feature high $b$ values because of the saturation in $m_b$:$M_0$ relations (Okal and Romanowicz, 1994). Similarly, high $b$ values have often been reported for seismicity induced either by mining (e.g. Kijko and Funk, 1994) or reservoir filling (e.g. Gough and Gough, 1970), but these may be affected by magnitude saturation. Nevertheless, we believe that our model for frequency–size relations of deep earthquakes provides some comparative insight for populations of volcanic events: many swarms of volcanic earthquakes originate in the country rock as a result of the overpressure owing to magma injection into the plumbing of the volcanic edifice; precise mapping of these swarms generally reveals three-dimensional clustering around the magma conduits (e.g. Klein et al., 1987). Such observations would suggest a seismogenic zone with a fractal dimension of three. On the other hand, volcanic events with lower $b$ values are generally interpreted as tectonic readjustments of the volcanic edifice during or after the eruption; these events have a tendency to be larger and to occur on well-defined fault planes, presumably with a fractal dimension of two. The difference in $b$ value between the two populations (which is an independent observation, more robust than the individual $b$ values, which could be affected by the particular magnitude used) would thus be easily explained from the difference in the fractal nature of the seismogenic zones of the two categories of earthquakes.

### 4.2. Saturation

As the size of the earthquake grows, the dimensions $W$ and/or $D$ will physically saturate, as the size of the seismogenic zone is finite. Several regimes of $\beta$ value could then arise depending whether one or both dimensions saturate, and whether the slip $\Delta u$ also saturates (following a '$W$' model in the terminology of Scholz (1982)) or keeps increasing (an '$L$' model). We propose here a two-stage saturation model (although emphasizing its speculative nature), to account for the various patterns observed in and outside Tonga.

(1) We propose that both transverse dimensions saturate, and that at least initially the slip keeps increasing ($L$ model). The seismogenic volume affected by the stress release then grows like $L$, and $M_0$ behaves as $L^2$, leading to $\beta = 1/2$. These assumptions remain tentative, but are supported by the observation (Apperson and Frohlich, 1987) that fault planes are not preferably oriented parallel to the down-dip or alongstrike directions of subduction, suggesting that

that both $W$ and $D$ saturate. The presence of non-double-couple components in deep earthquakes also favors this model (Houston, 1993). The other models (only one dimension saturating, and/or a saturation of $\Delta u$, would predict higher $\beta$ values (two thirds or unity)). This behavior is observed with a $\beta$ value (0.41) in reasonable agreement with the prediction (one-half) both in and outside Tonga. In particular, the sharp change of behavior in Tonga at $\log_{10} M_0 = 25.8$, featuring a decrease in $\beta$, rules out the $W$ model. We will denote this critical moment at which transverse saturation takes place by $M_{\mathrm{Low}}$ (see Fig. 7(a)).

(2) In an $L$ model, the slip $\Delta u$ keeps increasing, whereas the width $W$ of the fault is saturated. As a result, the stress drop $\Delta\sigma$ will increase with earthquake size. We further propose that, eventually, this increase is limited, and that the slip $\Delta u$ saturates, with the scaling then following the $W$ model. At this point, the moment will start growing like $L$, and the population should revert to $\beta = 1$. This behavior is observed outside Tonga for $\log_{10} M_0 \geq 25.9$. We will denote this critical moment at which slip saturation takes place by $M_{\mathrm{High}}$. The three-tier regime implied by this model is summarized in Fig. 7(a).

### 4.3. Summary

As documented in Figs. 7(b) and 7(c), the above model explains both the Tonga and non-Tonga populations, with the following provisions: (1) the critical moments $M_{\mathrm{Low}}$ and $M_{\mathrm{High}}$ are different in and outside Tonga because the dimensions of the seismogenic zones are much larger in Tonga, owing to the generally much cooler thermal structure, itself a reflection of the higher rate of subduction; (2) we do not observe the low-moment $\beta = 1$ regime outside Tonga because for these earthquakes $M_{\mathrm{Low}}$ is simply smaller than the CMT threshold of completeness; (3) we do not observe the high-moment $\beta = 1$ regime in Tonga, because the total number of such earthquakes over the 16 years of the CMT catalog is expected to be less than one.

Under those provisions, we can model the two populations as

$$\begin{aligned} \log_{10} N &= a_1 - \log_{10} M_0 \quad (M_0 \geq M_{\mathrm{High}}) \\ \log_{10} N &= a_2 - \frac{1}{2}\log_{10} M_0 \quad (M_{\mathrm{Low}} \leq M_0 \leq M_{\mathrm{High}}) \\ \log_{10} N &= a_3 - \log_{10} M_0 \quad (M_0 \leq M_{\mathrm{Low}}) \end{aligned} \tag{3}$$

with $M_{\mathrm{Low}} = 10^{25.7}$, $M_{\mathrm{High}} = 10^{26.8}$, $a_1 = 26.6$, $a_2 = 13.30$, and $a_3 = 26.1$ (Tonga), and $M_{\mathrm{Low}} \leq 10^{24}$, $M_{\mathrm{High}} = 10^{25.8}$, $a_1 = 26.9$, $a_2 = 14.1$, and $a_3 = 26.10$ (non-Tonga).

To discuss the last provision, we note that the nature of the two constants in Eq. (1) is fundamentally different: $\beta$, and hence the critical moments $M_{\mathrm{Low}}$ and $M_{\mathrm{High}}$ at which changes in $\beta$ take place, are 'intensive' variables related to the physical state of the slab, whereas $a$, and hence the $a_i$ values in (3), are 'extensive' variables characterizing the size of the populations sampled. In this respect, the value of $a_1$ in (3) is controlled by the total seismic moment released in the four-dimensional space–time window selected for study. By comparing the seismic moment release reported in the CMT catalog for Tonga at 500–600 km depth ($2.5 \times 10^{27}$ dyn cm) with the integral $\int_{M_0=M_{\min}}^{M_0=M_{\max}} M_0(-\mathrm{d}N)$ taken between appropriate bounds ($M_{\min} = 10^{24}$ dyn cm and $M_{\max} = 3 \times 10^{28}$ dyn cm, the moment of the recent Bolivian earthquake, the largest deep earthquake ever recorded), we find that (3) predicts $N = 0.58$ earthquakes with $M_0 \geq M_{\mathrm{High}}$ at 500–600 km depth in Tonga and during the period of the CMT dataset. This verifies that the high-moment $\beta = 1$ regime is not expected to be observed in the Tonga CMT dataset.

### 4.4. Model quantification

In this section, we attempt to quantify the model proposed above by providing estimates of physical parameters such as characteristic dimensions of seismogenic zones as they can be derived from the various critical moments, and to verify that they are acceptable in the context of available thermal models of the slabs.

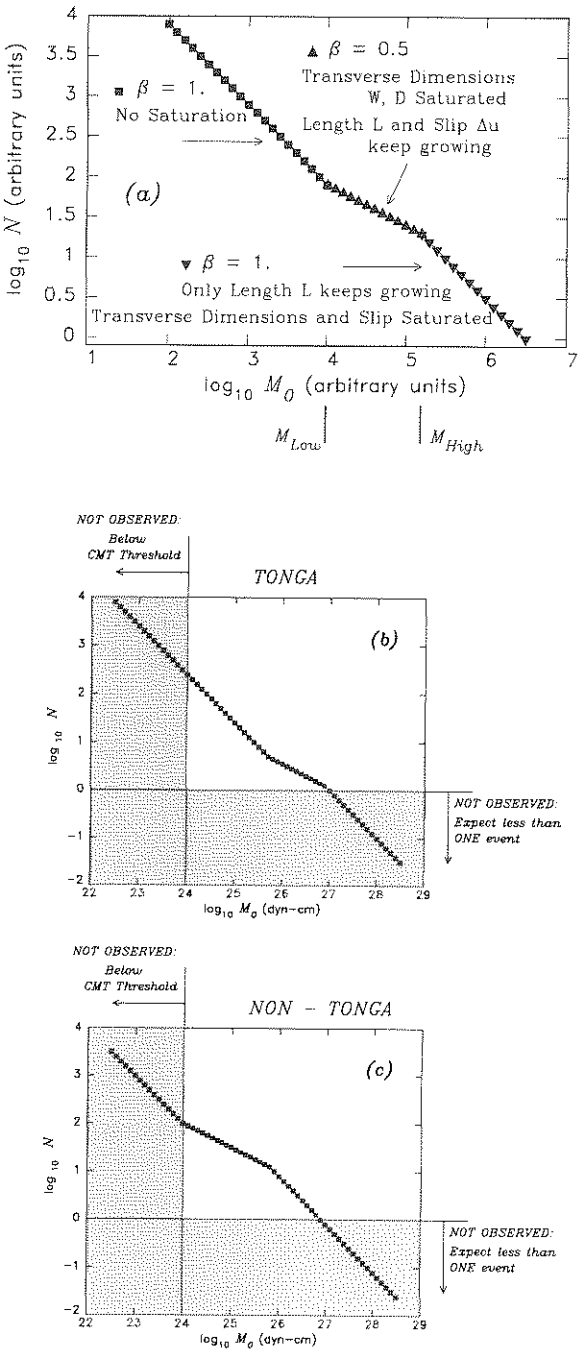


Fig. 7. (a) Expected three-regime behavior of size–moment relationships in the model proposed for deep earthquakes. The particular values of the locking constants on each axis would be controlled by the geometrical size of the seismogenic wedge (along the moment axis), and by the total level of seismic activity and the time window selected for analysis (population axis). (b), (c), Realistic models for Tonga (b) and non-Tonga (c) populations. These are obtained from (a) by using wedges of different sizes, which result in different corner moments, and imposing two observational constraints: the $10^{24}$ dyn cm CMT threshold of completeness, and the impossibility of observing fewer than one event over the lifespan of the CMT catalog. As a result, only the white quadrant is available for observation, and the two datasets exhibit markedly different behaviors.

In trying to interpret the critical moment $M_{Low}$ observed in Tonga as a function of the physical dimensions of the seismogenic zone, we use the expression

$$M_{Low} = \Delta\sigma W_S^3 \quad (4)$$

(e.g. Okal and Romanowicz, 1994), where $\Delta\sigma$ is the stress drop, assumed to be independent of earthquake size in the unsaturated regime. Stress drops are relatively poorly known, especially for deep earthquakes, and their estimates vary widely. Berckhemer and Jacob (1968) found relatively high values, of the order or 100–300 bars, as did Chung and Kanamori (1980) (60–500 bars), and more recently Fukao and Kikuchi (1987) (400–900 bars); all these studies consisted of modeling teleseismic P waves. On the other hand, Wyss and Molnar (1972) reported low values, of the order of 10–20 bars, and more recently Houston and Williams (1991) proposed values of 6–100 bars for deep earthquakes; in general, these studies relied on the concept of 'Orowan stress drop', which is computed from the ratio of seismic energy to seismic moment, and is expected to be less than the static stress drop (e.g. Houston, 1990). Also, the very high stress drops reported by Fukao and Kikuchi (1987) are computed for the largest subevent in the often complex source; it is not clear that these values could be applied to the whole source. Finally, the events in the former studies are usually larger than in the latter ones, which has led some workers to suggest that stress drops are higher for large earthquakes; there is, however, no evidence for such a systematic behavior in homogeneous datasets.

In the present study, we will use a value of 50–100 bars for $\Delta\sigma$, which is a reasonable average of the modeling studies. When applied to the critical moments of the 500–600 km and 600–650 km deep Tonga populations, this results in saturation widths, $W_S$, of 9–11 km and 4–5.5 km, respectively. These figures would be estimates of the transverse dimension of the seismogenic zone, beyond which the width $W$ of the fault cannot grow. It should be noted that Pacheco et al. (1992) have used a somewhat different geometry of faulting and a wide range of stress drops, together with a different value of $M_0^c$, to propose a saturating width of between 5 and 30 km. The tentative elbow around $4 \times 10^{24}$ dyn cm for the Tonga events deeper than 650 km would itself lead to a width $W_S$ of 3–4 km.

We interpret the $\beta = 1/2$ regime for small events outside Tonga by assuming that the critical moment for these events is lower than the threshold of completeness of our dataset, i.e. $10^{24}$ dyn cm. This would translate into $W_S \leqslant 2$–3 km.

Finally, we turn our attention to the $\beta = 1/2$ regimes (beyond $6 \times 10^{25}$ dyn cm in Tonga or between $10^{24}$ and $8 \times 10^{25}$ dyn cm outside Tonga). In this regime, we argue that the scaling follows an $L$ model, with the slip growing linearly with $L$, and consequently with $M_0^{1/2}$. As a result, one would expect the stress drop $\Delta\sigma$ to increase, outside Tonga, by a factor of approximately nine. Clearly, there is so much scatter in the stress drop values available in the literature that no argument can be made either for or against such a behavior. In the case of Tonga, the dataset covers only one order of magnitude of $M_0$, so that $\Delta\sigma$ would be expected to grow only by a factor of three, which is totally unresolvable at this stage.

## 5. Discussion and conclusion

We have shown in this paper that the distribution of earthquakes with size at the bottom of subduction zones is consistent with the idea that the seismogenic zone is three-dimensional, and that changes in $\beta$ value can be explained by relating them to changes in the scaling of the seismic source as it fills the transverse dimension of the seismogenic zone. This interpretation is mirrored on that used for shallow earthquakes (Rundle and Romanowicz, 1993), except for the different fractal nature of the zone. Differences between the regimes observed in and outside Tonga are attributable to the much faster pace of subduction at the Tonga trench.

The basic assumptions used in this paper (that deep earthquakes represent failure by faulting that fills a seismogenic volume, that Tonga has a greater thickness of seismogenic volume, and that differences in the observability of the three-regime behavior between Tonga and elsewhere stem

from differences in the rates of seismic moment release) are all consistent with a model explaining deep earthquakes in the context of phase changes (e.g. Kirby et al., 1991, 1995b). Whereas other models have been proposed to explain deep earthquakes (such as the persistence to great depths of hydrated phases), this theory assumes that deep seismic failure takes place by transformational faulting, a shear instability observed in the laboratory in minerals pressurized at low temperatures, so that the starting mineral is metastable while it is being deformed. Sudden failure occurs through the localization of phase transformation to a denser, fine-grained mineral (Durham et al., 1983; Kirby et al., 1985, 1991; Kirby, 1987; Green and Burnley, 1989; Burnley et al., 1991). This faulting behavior is thought to occur in olivine carried metastably into the field of spinel in the interiors of the coldest slabs. Simple theory (Sung and Burns, 1976) and recent thermokinetic models (Kirby et al., 1995b) predict that the region of olivine metastability should be wedge-shaped and that Tonga should have the thickest metastable wedge, as it is substantially colder than any other slab. Failure is restricted to the metastable wedge, because metastability is a necessary condition for transformational faulting. This model explains why failure by faulting occurs at all in the Earth's transition zone, and why deep earthquakes occur only in old, cold, slabs.

Fig. 8 presents a numerical modeling of the metastable wedge, using parameters simulating the geometry and kinematics of the Tonga slab (Kirby et al., 1995b). The various symbols identify several degrees of completion of the olivine-to-spinel transformation; they clearly show a wedge-like 'core' of metastable peridotite emplaced asymmetrically inside the slab, towards its upper (and hence colder) boundary. Except for the very tip of the wedge (below 650 km), the various curves are practically superimposed, defining sharp boundaries for the metastable field. The width of the metastable wedge is found to be approximately 23 km at 500 km, narrowing to 16 km at 600 km. The average value between 500 and 600 km (19 km) is somewhat larger than the estimate we derive in Section 4. At greater depths, the wedge further narrows, to about 5 km

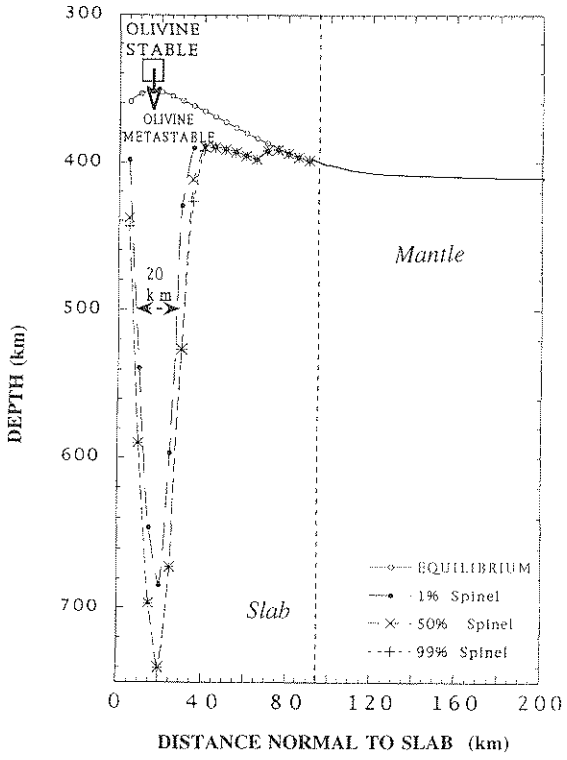


Fig. 8. Geometry of the metastable olivine wedge, predicted from a thermo-kinetic numerical simulation of the Tonga slab. For simplicity, the slab has been rotated vertical in the sketch, and occupies the left 95 km of the diagram. The continuous line in the mantle, prolonged by the open circles inside the slab, represents the line of olivine–spinel equilibrium. Inside the slab, the lower temperatures affect the kinetics of the reaction, and various symbols are used to map various levels of completion of the phase transformation. The metastable wedge has sharp lateral boundaries and is found to be about 20 km in width at 500 km depth. After Kirby et al. (1995b).

at 650 km (for the zone in which only 1% has transformed to spinel), in agreement with our tentative results based on the evolution of the $\beta$ value at those depths.

The sharp boundaries of the metastable zone are expected to be the site of significant stress, arising from the differences in density between the metastable and transformed mineral assemblages. One would then expect that seismicity would develop preferentially along these lines. This is in general agreement with the observation in the Tonga subduction zone of 'double Benioff zones', separated by 25 km, by Wiens et al. (1993).

As these workers' observations were made at significantly shallower depths (typically between 350 and 450 km), they are in good agreement with the model of Fig. 8. Also, this preferential occurrence of seismicity at the edges of the metastable wedge may help explain the discrepancy with the size of the seismogenic zone derived from the present study, as the saturation of source growth will be more pronounced towards the side of the metastable wedge than towards the center of the wedge, and hence will start at lower values of the seismic moment.

If the moment production rate is proportional to the rate of creation of metastable olivine, then the high descent rate and thicker metastable wedge in Tonga should produce a larger long-term moment release (per unit length along the strike of the slab). As detailed in Section 4, this is easily verified from the CMT catalog.

Finally, it is also interesting to note that intermediate depth seismicity (say in the 200–300 and 300–400 km bins) outside Tonga, and the deep activity in Tonga exhibit different population–moment relationships, whereas the temperature in the two regions may be expected to be comparable (Furukawa, 1994). This is easily explained in the framework of transformational faulting, as metastability cannot take place above 400 km in a hot slab, and thus the intermediate earthquakes, which cannot be due to transformational faulting, must involve a different process.

### *5.1. The case of the great 1994 deep earthquakes—Fiji and Bolivia*

In this section, we wish to discuss the two great deep earthquakes of 1994: the 9 March event in Fiji ($h = 564$ km; $M_0 = 3 \times 10^{27}$ dyn cm), and the 9 June event in Bolivia ($h = 637$ km; $M_0 = 3 \times 10^{28}$ dyn cm), in the context of our present study.

#### *5.1.1. Fiji, 9 March 1994*

From the standpoint of its moment, the Fiji event was for 3 months (until the occurrence of the even bigger Bolivian shock) the largest deep event known since the inception of the CMT catalog; it was also five times larger than its regional runner-up in the catalog (26 May 1986; $5.6 \times 10^{26}$ dyn cm), serving proof that very large deep earthquakes do occur in the Tonga–Fiji area. Preliminary results relating to the World Wide Standardized Seismograph Network (WWSSN) years (1962–1971) do not affect the singular character of the 1994 event, as the largest deep earthquake in Tonga for that period was the 9 October 1967 shock ($h = 654$ km; $M_0 = 6 \times 10^{26}$ dyn cm) (Sasatani, 1976; Huang et al., 1994), and in the 500–600 km range, the 25 August 1963 earthquake ($h = 599$ km; $M_0 = 3.8 \times 10^{26}$ dyn cm). However, from Eq. (3), the expected number of events as large as, or bigger than, the 1994 Fiji earthquake is a mere 0.25 over the lifetime of the CMT project (16 years); alternatively, the repeat time of such an event would be predicted at 64 years. It is remarkable that an apparently very large deep earthquake ($h \approx 560$ km) with Pasadena magnitude $M_{PAS} = 7.9$ (Gutenberg and Richter, 1954) did indeed occur south of Fiji on 26 May 1932 (Brunner, 1938); preliminary estimates would make it comparable in size with the 1994 Fiji shock (W.-C. Huang, personal communication, 1994). In short, the occurrence of the 1994 event and its moment fit our model well, and should not be considered anomalous, a conclusion also reached by Giardini and Lundgren (1994).

A significant problem arises, however, from the size and orientation of its rupture area: both the locus of rupture during the main shock and the distribution of aftershocks extend beyond the active seismic zone (McGuire et al., 1994; Wiens et al., 1994), suggesting that seismogenic rupture did indeed take place in material otherwise considered aseismic, based on the geometry of the Wadati–Benioff zone. This situation is in itself a challenge to any theory of the mechanism of deep seismicity.

#### *5.1.2. Bolivia, 9 June 1994*

On the other hand, the Bolivian earthquake took place in a three-dimensional domain previously considered aseismic, with the nearest documented seismicity (the 15 August 1963 earthquake) located 178 km away. Detection capabilities varied in the past decades, but our experience (Okal and Bina, 1994) shows that the area

remained aseismic at the level of $M_0 = 2 \times 10^{23}$ dyn cm (approximately $m_b = 4.8$) since 1963, and $M_0 = 10^{25}$ dyn cm (approximately $M_{PAS} = 6$) since 1920. Similarly, the Bolivian earthquake featured three teleseismically recorded aftershocks in the first 45 days (and 20 more located by a dense portable array) (Wiens et al., 1994; S.L. Beck, personal communication, 1995). Hundreds to thousands of such aftershocks would have been expected from a shallow event of comparable size, and for that matter, 84 were observed after the Fiji earthquake, whose moment was ten times smaller. This situation is exceptional, but not unique, as the 1970 Colombian earthquake to the north, the two deep northern Peruvian shocks of 1921–1922, and to a great extent, the Spanish earthquake of 1954 were also similarly isolated, both in space and time (Giardini and Lundgren, 1994; Okal and Bina, 1994). In the presence of a single large mainshock, it is of course impossible to attempt any kind of frequency–moment modeling, and it is clear that the regime of seismogenesis in such regions must differ significantly from that in other portions of subducted slabs.

The question of the size of the source of the Bolivian earthquake in relation to the structure of the slab is also of some interest: most detailed studies of the source region describe it as subhorizontal with dimensions of 50 km by 50 km, although Huang and Chen (1994) proposed that it may consist of several en-échelon segments, with a transverse dimension of no more than 20 km. These estimates are not incompatible with the model of a metastable wedge, if one assumes that the deformation of the slab in the epicentral region (evidenced from the large geometrical offset between the northern and southern segments of the Wadati–Benioff zone) is accompanied by a thickening of the slab, as suggested by preliminary models of seismic tomography in the region (Engdahl et al., 1995; Kirby et al., 1995a).

In conclusion, both the Fiji and Bolivia events present formidable challenges to any modeling of deep seismicity, but for different reasons: the moment of the Fiji earthquake was not unexpected but its geometry transcends the documented Wadati–Benioff zone; on the other hand, the Bolivian shock may fit inside an adequately thickened metastable wedge, but its size and uniqueness remain unexplained. Gigantic deep events may be in a class by themselves, which may not lend itself to the basic principle of scale invariance underlying population models. A similar situation may indeed exist for the very largest shallow earthquakes, as in the case of the 1960 Chilean event, whose model generally includes a gigantic precursory component, extending to depths greater than 100 km, where the nature of the seismic rupture may differ from its shallow counterpart, as evidenced by the extremely slow character of the precursor (Cifuentes and Silver, 1989).

In summary, the basic results of the present analysis, that (1) deep zones of seismogenesis are inferred to be three-dimensional, (2) the Tonga seismogenic zone is significantly thicker than others, and (3) the moment productivity (per unit length along the strike of the slab) is greater in Tonga, are all expected from the metastability theory. This theory also explains two of the most striking, robust, and long-observed features of global deep seismicity, namely that Tonga produces more deep earthquakes than any other slab, but that large deep earthquakes are less frequent in Tonga than in other deep subduction zones. Although not strictly requiring transformational faulting, or offering a proof of its occurrence in deep slabs, our results are easily explained in the framework of that theory, and therefore generally support its concepts, including the order of magnitude of the size of the metastable wedge.

## Acknowledgments

We thank E.R. Engdahl, A. McGarr, D.A. Wiens, S.L. Beck, and W.-C. Huang for many discussions and for providing results before publication. This research was supported in part by the National Science Foundation under Grant EAR-93-16396 (E.A.O.).

## References

Apperson, K.D. and Frohlich, C.H., 1987. The relationship between Wadati–Benioff zone geometry and the *P*, *T* and

*B* axes of intermediate and deep-focus earthquakes. J. Geophys. Res., 92: 13821–13831.

Berckhemer, H. and Jacob, K.H., 1968. Investigation of the dynamical process in earthquake foci by analysing the pulse shape of body waves. Final Sci. Rep., Contract AF61 (052)-801, University of Frankfurt, 85 pp.

Bevis, M., Schutz, B.E., Taylor, F.W., Stowell, J., Perin, B., Recy, J. and Isacks, B.L., 1991. Crustal motions observed near the Tonga trench (1988–1990). Eos, Trans. Am. Geophys. Union, 72(44): 115 (abstract).

Bevis, M., Taylor, F.W., Schutz, B.E. and Calmant, S., 1993. Geodetic observations of convergence and back-arc spreading in the S.W. Pacific. Eos, Trans. Am. Geophys. Union, 74(43): 60 (abstract).

Brunner, G.J., 1938. The deep earthquake of May 26, 1932 near the Kermadec Islands, Gerlands Beitr. Geophys. 53: 1–64.

Burnley, P.C., Green, II, H.W. and Prior, D., 1991. Faulting associated with the olivine-to-spinel transformation in $Mg_2GeO_4$ and its applications for deep-focus earthquakes. J. Geophys. Res., 96: 425–443.

Burr, N.C. and Solomon, S.C., 1978. The relationship of source parameters of oceanic transform earthquakes to plate velocity and transform length. J. Geophys. Res., 83: 1193–1200.

Chung, W.-Y. and Kanamori, H., 1980. Variation of seismic source parameters and stress drops within a descending slab and its implication in plate mechanics. Phys. Earth Planet. Inter., 23: 134–159.

Cifuentes, I.L. and Silver, P.G., 1989. Low-frequency source characteristics of the great 1960 Chilean earthquake. J. Geophys. Res., 94: 643–663.

Durham, W., Heard, H. and Kirby, S.H., 1983. Experimental deformation of polycrystalline ice: preliminary results. J. Geophys. Res., 88: 377–392.

Engdahl, E.R., van der Hilst, R.D. and Berrocal, J. 1995. Tomographic imaging of subducted lithosphere beneath South America: implications for the June 9, 1994 deep Bolivia earthquake. Geophys. Res. Lett., in press.

Engebretson, D.C., Mammerickx, J. and Raymond, C.A., 1991. Tonga lineations: the Phoenix plate has arisen? Eos, Trans. Am. Geophys. Union, 72(43): 444 (abstract).

Frohlich, C. and Apperson, D.K., 1992. Earthquake focal mechanisms, moment tensors, and the consistency of seismic activity near plate boundaries. Tectonics, 11: 279–296.

Frohlich, C. and Davis, S.D., 1993. Teleseismic *b*-values; or, much ado about 1.0. J. Geophys. Res., 98: 631–644.

Furukawa, Y., 1994. Two types of deep seismicity in subducting slabs. Geophys. Res. Lett., 20: 1181–1184.

Fukao, Y. and Kikuchi, M., 1987. Source retrieval for mantle earthquakes by iterative deconvolution of long-period *P* waves. Tectonophysics, 144: 249–269.

Geller, R.J., 1976. Scaling relations for earthquake source parameters and magnitudes. Bull. Seismol. Soc. Am., 66: 1501–1523.

Giardini, D., 1988. Frequency distribution and quantification of deep earthquakes. J. Geophys. Res., 93: 2095–2105.

Giardini, D. and Lundgren, P.R., 1994. Expected and unexpected source characteristics of the June 9, 1994 deep Bolivia earthquake. Eos, Trans. Am. Geophys. Union, 75(44): 466 (abstract).

Gough, D.I. and Gough, W.I., 1970. Load-induced earthquakes at Lake Kariba—II. Geophys. J.R. Astron. Soc., 21: 79–101.

Gutenberg, B. and Richter, C.F., 1954. Seismicity of the Earth. Princeton University Press, Princeton, NJ, 310 pp.

Houston, H., 1987. Source characteristics of large earthquakes at short periods. Ph.D. Thesis, California Institute of Technology, Pasadena, 148 pp.

Green, II, H.W. and Burnley, P.C., 1989. A new self-organizing mechanism for deep earthquakes. Nature, 341: 733–737.

Houston, H., 1990. Broadband source spectrum, seismic energy, and stress drop of the 1989 Macquarie Ridge earthquake. Geophys. Res. Lett., 17: 1021–1024.

Houston, H., 1993. The non-double-couple component of deep earthquakes and the width of the seismogenic zone. Geophys. Res. Lett., 20: 1687–1690.

Houston, H. and Williams, Q., 1991. Fast rise times and the mechanism of deep earthquakes. Nature, 352: 520–522.

Huang, B.-S. and Chen, W.-P., 1994. Directivity of the June 9, 1994 deep Bolivia earthquake: a case of en-échelon rupture. Eos, Trans. Am. Geophys. Union, 75(44): 466 (abstract).

Huang, W.-C., Okal, E.A., Ekström, G. and Salganik, M.P., 1994. CMT inversion of analog seismograms of deep earthquakes: progress report on the WWSSN era. Seismol. Res. Lett., 65: 65 (abstract).

Kijko, A. and Funk, C.W., 1994. The assessment of seismic hazards in mines. J. S. Afr. Inst. Min. Metall., 94: July, 179–185.

Kirby, S.H., 1987. Localized polymorphic phase transitions in high-pressure faults and applications to the physical mechanism of deep earthquakes. J. Geophys. Res., 92: 13789–13800.

Kirby, S.H., Durham, W.B. and Heard, H.C., 1985. Rheology of ices $I_h$, II and III at high pressure: a progress report. In: J. Klinger, D. Benest, A. Dollfus and R. Smoluchowski (Editors), Ices in the Solar System, Reidel, Dordrecht, pp. 711–729.

Kirby, S.H., Durham, W.B. and Stern, L.A., 1991. Mantle phase changes and deep-earthquake faulting in subducting lithosphere. Science, 252: 216–225.

Kirby, S.H., Okal, E.A. and Engdahl, E.R., 1995a. The 09 June 1994 great Bolivian deep earthquake: An exceptional deep earthquake in an extraordinary subduction zone. Geophys. Res. Lett., in press.

Kirby, S.H., Stein, S., Okal, E.A. and Rubie, D., 1995b. Deep earthquakes and metastable mantle phase transformations in subducting oceanic lithosphere, Revs. Geophys. Space Phys., submitted.

Klein, F.W., Koyanagi, R.Y., Nakata, J.S. and Tanigawa, W.R., 1987. The seismicity of Kilauea's magma system, US. Geol. Surv. Prof. Pap., 1350: 1019–1185.

McGuire, J.J., Wiens, D.A., Shore, P.J., Bevis, M.G., Draunidalo, K., Prasad, G. and Helu, S.P., 1994. Rupture properties of the March 9, 1994 deep Tonga earthquake and its aftershocks. Eos, Trans. Am. Geophys. Union, 75(44), 466 (abstract).

Minakami, T., 1974. Seismology of volcanoes in Japan. In: L. Civetta, P. Gasparini, G. Luongo and A. Rapolla (Editors), Physical Volcanology. Elsevier, Amsterdam, pp. 1–27.

Molnar, P., 1979. Earthquake recurrence intervals and plate tectonics. Bull. Seismol. Soc. Am., 69: 115–133.

Okal, E.A., 1992. Use of the mantle magnitude $M_m$ for the reassessment of the seismic moment of historical earthquakes. II. Intermediate and deep events. Pure Appl. Geophys., 139: 59–85.

Okal, E.A. and Bina, C.R., 1994. The deep earthquakes of 1921–1922 in Northern Peru. Phys. Earth Planet. Inter., 87: 33–54.

Okal, E.A. and Romanowicz, B.A., 1994. On the variation of *b*-values with earthquake size. Phys. Earth Planet. Inter., 87: 55–76.

Okal, E.A. and Stein, S., 1987. The 1942 Southwest Indian Ocean Ridge earthquake: largest ever recorded on an oceanic transform. Geophys. Res. Lett., 14: 147–150.

Pacheco, J.F., Scholz, C.H. and Sykes, L.R., 1992. Changes in frequency-size relationship from small to large earthquakes. Nature, 355: 71–73.

Romanowicz, B.A. and Rundle, J.B., 1993. On scaling relations for large earthquakes. Bull. Seismol. Soc. Am., 83: 1294–1297.

Rundle, J.B., 1989. Derivation of the complete Gutenberg–Richter magnitude–frequency relation using the principle of scale invariance. J. Geophys. Res., 94: 12337–12342.

Sasatani, T., 1976. Focal process of the Tonga deep-focus earthquake of 1967. Zisin. Bull. Seismol. Soc. Japan; Supp. Annu. Mtg. 29, p. 101 (abstract; in Japanese).

Scholz, C.H., 1982. Scaling laws for large earthquakes: consequences for physical models. Bull. Seismol. Soc. Am., 72: 1–14.

Sung, C.M. and Burns, R.G., 1976. Kinetics of the olivine–spinel transition: implications to deep-focus earthquake genesis. Earth Planet. Sci. Lett., 32: 165–170.

Talandier, J. and Okal, E.A., 1987. Seismic detection of underwater volcanism: the example of French Polynesia. Pure Appl. Geophys., 125: 919–950.

Turcotte, D.L., 1992. Fractals and Chaos in Geology and Geophysics, Cambridge University Press, Cambridge, 221 pp.

Wiens, D.A., McGuire, J.J. and Shore, P.J., 1993. Evidence for transformational faulting from a deep double seismic zone in Tonga. Nature, 365: 790–793.

Wiens, D.A., McGuire, J.J., Shore, P.J., Bevis, M.G., Draunidalo, K., Prasad, G. and Helu, S.P., 1994. A deep aftershock sequence and implications for the rupture mechanism of deep earthquakes. Nature, 372: 540–543.

Willemann, R.J. and Frohlich, C.F., 1987. Spatial patterns of aftershocks of deep-focus earthquakes. J. Geophys. Res., 92: 13927–13943.

Wyss, M. and Molnar, P., 1972. Source parameters of intermediate and deep focus earthquakes in the Tonga arc. Phys. Earth Planet. Inter., 6: 279–292.